Reprinted from Applied Optics, Vol. 25, Page 2158, July 1, 1986

Analysis of image noise due to position errors in laser writers

Peter D. Burns, Majid Rabbani, and Lawrence A. Ray

For raster-written images, the modulated laser exposing beam is scanned across the photosensitive material in a line-by-line configuration. Image noise can be introduced by the writer directly, for example, by the granularity of the photosensitive materials and indirectly, for example, by beam position errors. For analysis of the effect of position errors they must first be related to their resultant exposure fluctuations. Here, position errors are addressed via models of image writing that include several spot/pixel writing schemes. Three types of image noise due to page-scan position error are examined. The effect of low-frequency position errors is described. Exposure fluctuations due to broadband stochastic errors are then addressed. For laser writers using a rotating polygon for beam deflection, the effect of stochastic facet-angle errors is repeated down the image; this results in periodic exposure fluctuations and is the third type of image noise analyzed. Expressions are given for the mean and variance of the exposure error in terms of the statistics of the position error, writing spot profile, and raster sampling distance. The analytical models are then compared with the results of an image simulation calculation. In this way, the exposure error fluctuations are described by their noise power spectra as functions of spatial frequency. After consideration of the sensitometry of the hardcopy recording materials, the exposure errors are then related to the corresponding output density fluctuations.

I. Introduction

Most laser image writers scan the laser light source across the photosensitive material in a line-by-line, or raster, format, which is well suited to both continuous tone and text imaging.[1] The exposing beam is deflected across the photosensitive material, while the materials are moved incrementally in the orthogonal direction, for each raster line. The beam intensity is modulated at discrete intervals corresponding to the intended optical density of each pixel in the final image. Reference 1 gives more details of various deflection schemes. This process can be thought of as a conversion of the image from a 1-D sampled digital sequence to a 2-D continuous representation.

The design of a laser writer places limitations on this conversion from discrete to continuous form that introduce error or image noise. Consider, for example, the case where the discrete signal is merely a sampled version of an input optical image. The corresponding written image will contain fluctuations attributable to the finite number of levels (bits) used for the discrete sampled image. Other sources of image noise introduced by the image writer are stochastic variations in the laser beam intensity, granularity of the photosensitive material, and beam position (or velocity) errors. The first two noise sources can be analyzed by considering the signal and noise transfer during modulation and image writing. Position errors, however, must first be related to their resultant output exposure fluctuations. Our focus is on errors that occur in the slow or page scan direction causing the line pitch to vary.

Since the written exposure image is dependent on the repeated raster scanning of the laser, errors in the line position degrade image quality. This occurs with the introduction of 1-D banding and streak artifacts which will be most evident in the constant or low-contrast image areas. Often the design goal is to set position error tolerance values so that no banding artifacts are visible under normal viewing conditions. These tolerance levels vary due to several factors, e.g., pixel writing configuration, contrast of the recording material, and nature of the position errors. Bestenreiner *et al.*[2] have investigated the effect of periodic line position errors on the reproduction of halftone and continuous-tone recording processes. They found that viewers could detect the presence of low-frequency periodic image fluctuations due to fractional position errors of 1%. The sensitivity of human vision to

The authors are with Eastman Kodak Company, Research Laboratories, Rochester, New York 14650.
Received 6 December 1985.
0003-6935/86/132158-11$02.00/0.

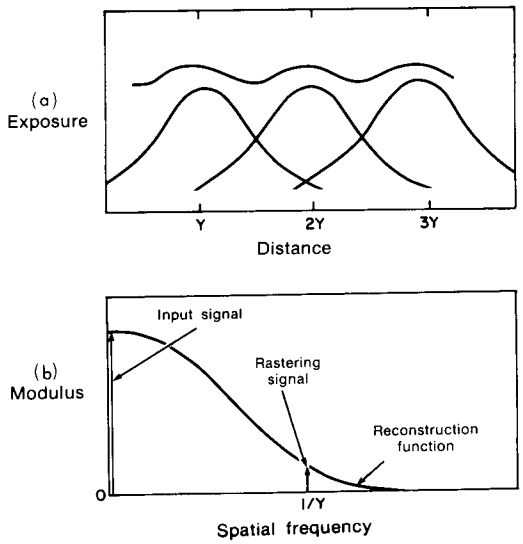

Fig. 1. (a) Effect of overlapping exposure beams corresponding to a constant input signal. (b) Frequency domain representation of above. The constant input is aliased at $1/Y$, since the reconstruction function is not bandlimited.

these artifacts, however, will strongly depend on the spatial frequency of their components.[3]

Laser writers have several sources of position errors, and rarely do current designs meet such stringent tolerances. Values of 5–20% are typical. Kessler and Shack[4] describe measurement of several sources for laser printers using a polygon spinner for beam deflection. Scanning accuracy for galvanometer deflectors has been addressed by Brosens.[5] Many applications require a secondary correcting deflector to compensate for systematic line-position errors.[2,6] Although the original uncompensated position errors may be known or periodic, the residual errors after compensation will often contain stochastic components.

To date, no general analysis of image noise due to raster-line position errors is available. This work addresses the effect of periodic and stochastic position errors and explicitly includes the effect of the modulated laser beam shape. The objective is to provide physical understanding of the effect on the image that can be related to other imaging characteristics of the laser printer, such as mean density, contrast, and MTF.

II. Low-Frequency Position Errors

We start by assuming that we are printing a uniform image area at some signal level with no position errors as in Fig. 1(a). When images are sampled and reconstructed, they are subject to both filtering (blurring) and aliasing.[7,8] Rastering is an example of aliasing where the zero-frequency mean signal is aliased at the sampling frequency, as shown in Fig. 1(b). For a constant input exposure I, the written output exposure is

$$C(x) = I + 2IR(1/Y)\cos(2\pi x/Y), \tag{1}$$

where Y is the constant line-pitch distance, and $R(f)$ is the Fourier transform of the spot profile. Here we assume that the rastering components at multiples of the sampling frequency are negligible. Note that this periodic fluctuation has a high spatial frequency, twice the Nyquist frequency, and is usually not in a region of high visual sensitivity. We address it here recognizing that this component is present in a written image in the absence of position errors. Fluctuations in images due to position errors will be considered separately from fluctuations due to other causes.

For many systems the reconstruction function R limits signal modulation and, therefore, is equal to the MTF. However, since other transfer functions (filters) can be operating on the signal, we will not refer to R as the system MTF. The output exposure is the desired constant plus a raster cosine signal. The average exposure C can be written as a function of beam velocity or line pitch:

$$\begin{aligned} C(\text{ergs/cm}^2\,\text{s}) &= \frac{J(\text{ergs/cm s}^2)}{s(\text{cm/s})}, \\ C(\text{ergs/cm}^2\,\text{s}) &= \frac{K(\text{ergs/cm s})}{Y(\text{cm})}, \end{aligned} \tag{2}$$

where s is the fast scan beam velocity, and J, K are constant scale factors dependent on the exposure source and optics.

Consider the effect of low-amplitude low-frequency (temporal and spatial) errors that cause the line pitch to vary across the image. Now Y can be a random variable. Combining Eqs. (1) and (2),

$$\tilde{C}(x) = \frac{K}{\tilde{Y}} + \frac{2K}{\tilde{Y}} R(1/\tilde{Y})\cos(2\pi x/\tilde{Y}), \tag{3}$$

where the tilde indicates a random variable. Equation (3) shows that both the mean exposure and periodic raster ripple will be functions of the varying line pitch. Ignoring the second term of Eq. (3), the variation in exposure due to low-frequency stochastic position error can be expressed as

$$\frac{\sigma_C}{C} = K\frac{\sigma_Y}{Y}, \tag{4}$$

where C and Y are now mean values. The same result holds for low-frequency sinusoidal position error due to, for example, stage flutter:

$$\frac{\Delta C}{C} = K\frac{\Delta Y}{Y}, \tag{5}$$

where ΔY is the sinusoidal position error. Equations (4) and (5) show that the result of low-frequency random or sinusoidal position errors is a corresponding proportional error in output exposure.

III. Random Line-Position Errors

We now turn to the analysis of random line-position errors. Here we assume that the errors in raster positions are independent, so structured errors such as those generated from a rotating polygon or periodic vibration are excluded. The natural shape of the laser spot is a Gaussian profile; however, by using masks the shape of the spot can be altered. The work of Lee,[9] Ray,[10] and Sullivan[11] describes this process and its motivation. The pyramid, or linear interpolator (LI), profile is important because of both reduced signal aliasing and no raster ripple component. Consequently, we consider the effect of a chosen beam shape on exposure fluctuations because of the random position errors.

Model

Our model as above is one-dimensional, since the errors are assumed to be mislocations of the raster lines and not individual pixels. For a constant digital signal, the ideal reconstructed exposure is

$$C(x) = \sum_{i=-\infty}^{\infty} S_i(x), \tag{6}$$

where $S(x)$ is the spot profile in the slow scan direction. The corrupted noisy exposure because of position errors is

$$C_{\text{noisy}}(x) = \sum_{i=-\infty}^{\infty} S_i(x + z_i), \tag{7}$$

where $\{z_i\}$ are independent identically distributed (iid) random variables with zero mean.

The exposure error introduced by the position error is given by the difference in Eqs. (6) and (7):

$$\begin{aligned} v(x) &= C(x) - C_{\text{noisy}}(x) \\ &= \sum_{i=-\infty}^{\infty} [S_i(x) - S_i(x + z_i)]. \end{aligned} \tag{8}$$

The function $v(x)$ will be referred to as the error function. The error function will now be analyzed to determine the statistics of the error and image exposure fluctuations that would be expected from typical realizations of such position errors. Our analysis will be general in form but will focus on the case of Gaussian and linear interpolator (triangular) beam profiles.

Let us assume that the laser writing device is unable to maintain perfect (constant) raster spacing; then the flat exposure level shown in Fig. 2(a), for a linear interpolator spot, becomes more like the exposure of Fig. 2(b). The error function that describes the image exposure fluctuations due to position errors is shown in Fig. 2(c). The image will appear as a field of darker and lighter stripes. Our approach is to derive expressions for the mean and variance of the exposure error functions for both spot shapes. The derivations of the results are in Appendix A.

Gaussian Profile

For images written with a Gaussian beam, the ideal exposure will naturally contain a periodic raster ripple.

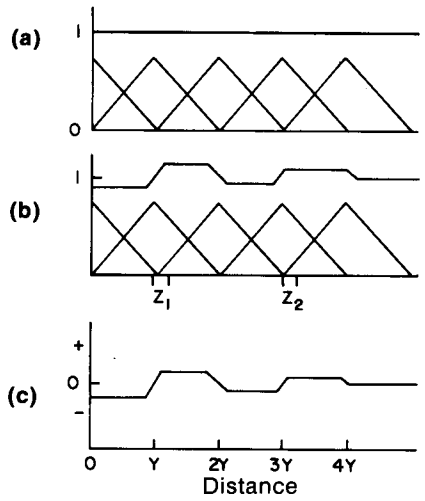

Fig. 2. Written exposure for a constant input of a spot with the linear-interpolator (triangular) shape (a) without position error, (b) with error, (c) error exposure signal v.

Despite this, the Gaussian beam is used in most writing devices. The error function of Eq. (8) does not include this fluctuation, since it occurs in the absence of position errors. The Gaussian spot profile in the slow scan direction for a raster position iY is given by

$$S_i(x) = \exp\left[-\tfrac{1}{2}\left(\frac{x - iY}{\sigma_y}\right)^2\right]. \tag{9}$$

(For the remainder, i represents an index parameter, and j denotes $\sqrt{-1}$.)

We assume that the signal to be written is a uniform field of unit intensity and that the misplacement errors z_i are iid normal random variables with zero mean and variance σ_z^2. Theorems 1 and 2 (see Appendix A) establish the first- and second-order moments of the error function $v(x)$. The mean error at position x is $\mu_v(x) = E[v(x)] =$

$$\sum_{i=-\infty}^{\infty} \left(S_i(x) - \frac{\sigma_y}{\sqrt{\sigma_y^2 + \sigma_z^2}} \exp\left\{-\tfrac{1}{2}\left[\frac{(x - iY)^2}{\sigma_y^2 + \sigma_z^2}\right]\right\} \right), \tag{10}$$

where σ_y is the (standard deviation) shape parameter of the Gaussian spot, and σ_z^2 is the variance of the position-error probability density function (pdf). Note that $\mu_v(x)$ is not stationary but is periodic with a period equal to the raster width Y (Fig. 3). The following heuristic argument might be helpful in explaining the nonstationary behavior of the error. Consider the output exposure at the raster position $x = iY$. The major contribution to this output comes from the Gaussian spot centered at that point. Shifting the spot profile in either direction will result in a lower output as the Guassian falls off sharply. An equivalent exposure error at a nearby raster line will not restore the exposure at this point as the slope of the tail of the Gaussian will be nearly zero. This implies that regardless of the direction of the random displacement, the error function will most likely be negative. The situation at midpoints between raster lines is re-

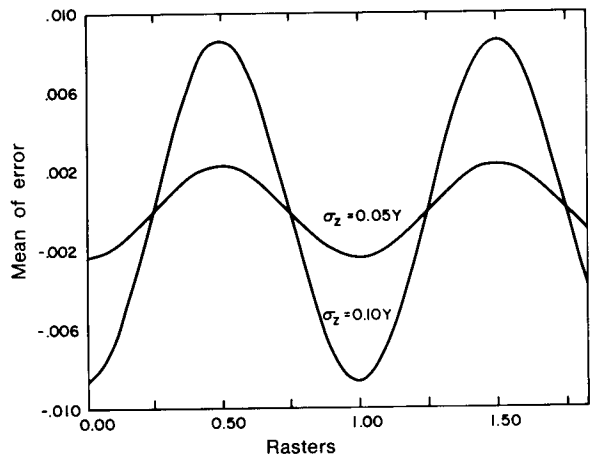

Fig. 3. Calculated mean exposure error for a Gaussian beam with $\sigma_y = 0.44Y$.

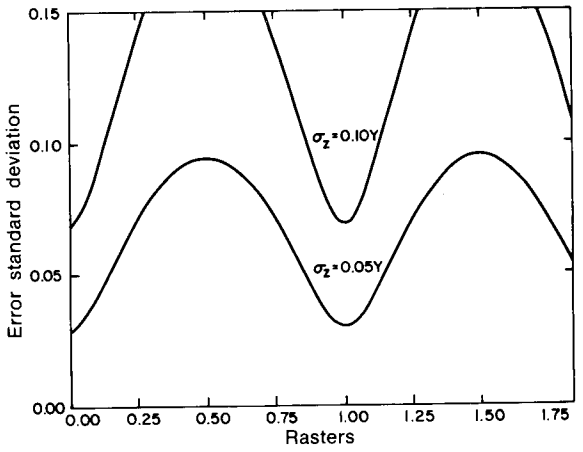

Fig. 4. Calculated standard deviation of exposure error for Gaussian beam with $\sigma_y = 0.44Y$.

versed. This causes a bias in the error, which will be a function of position.

The mean exposure error given by Eq. (10) can also be expressed in terms of the Fourier transform of the beam profile. As shown in Appendix B, the first-order approximation to the mean exposure error is

$$\mu_v(x) = K \cdot \frac{\sigma_z^2}{Y^3} \cdot R(1/Y) \cos(2\pi x/Y), \tag{11}$$

where K is a constant and R is the Fourier transform of the spot profile. We note that this error is proportional to the position-error variance, not the standard deviation. As the spot profile is made narrower, $R(f)$ becomes wider in spatial frequency, and so the value of $R(1/Y)$ is increased. Thus the amplitude of the mean exposure fluctuations is increased. The nonstationary mean of the exposure error for a Gaussian spot has the effect of adding a periodic component at the raster frequency $(1/Y)$. The component has a small amplitude and is opposite in sign to the raster ripple described in Eq. (1).

We now address the variance of the error function. From Theorem 2, this is given by

$$\sigma_v^2(x) = E\{[v(x) - \mu_v(x)]^2\}$$

$$= \sum_{i=-\infty}^{\infty} \left\{ \frac{\sigma_y}{(2\sigma_z^2 + \sigma_y^2)^{1/2}} \exp\left[-\frac{(x - iY)^2}{2\sigma_z^2 + \sigma_y^2} \right] \right.$$

$$\left. - \frac{\sigma_y^2}{\sigma_y^2 + \sigma_z^2} \exp\left[-\frac{(x - iY)^2}{\sigma_y^2 + \sigma_z^2} \right] \right\}. \tag{12}$$

Figure 4 shows the standard deviation at interraster positions. The standard deviation increases with increasing σ_z as would be expected.

The width of the Gaussian profile has a marked effect on the mean and variance of the error. A larger-width Gaussian profile will have smaller error means and variances. Figure 5 shows this relationship for four Gaussian profiles. These results can be understood by analyzing the error process as a function of spatial frequency. A derivation for the noise power spectrum of the exposure error is given in Appendix C.

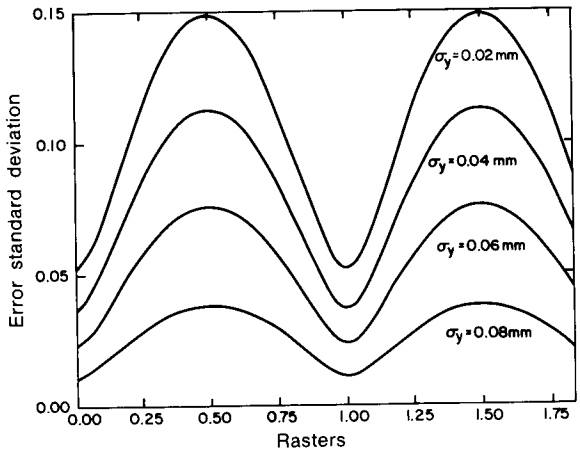

Fig. 5. Calculated standard deviations of exposure error for various Gaussian beam widths; position error has standard deviation $\sigma_z = 0.01Y$.

$$PS(f) = [K\sigma_z f R(f)]^2, \tag{13}$$

where K is a constant and R is the Fourier transform of the spot profile. As the spot profile is increased, $R(f)$ increases resulting in a higher noise power spectrum. The error exposure variance is increased, since it is equal to the integral of the noise power spectrum. The noise power spectrum will be discussed further in Sec. IV along with the simulation results.

The natural conclusion is to design the laser writing system with a wider Gaussian profile. This conclusion must be balanced with the knowledge that the wider Gaussian profile will diminish the modulation transfer bandwidth of the laser writer. In fact, the higher MTF of a system employing a narrow Gaussian beam partially explains the increased sensitivity to raster errors. Aside from this, all examples use a Gaussian profile with the $\sigma_y = 0.44$ raster widths. This was selected because it closely matches the reconstruction function of the linear interpolator.[11]

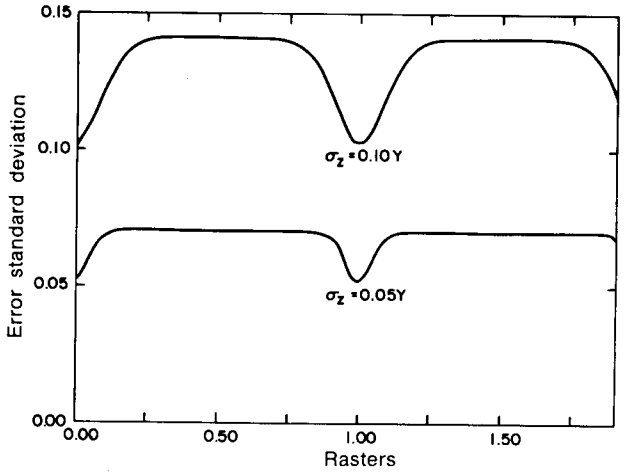

Fig. 6. Standard deviation of exposure error for linear interpolator.

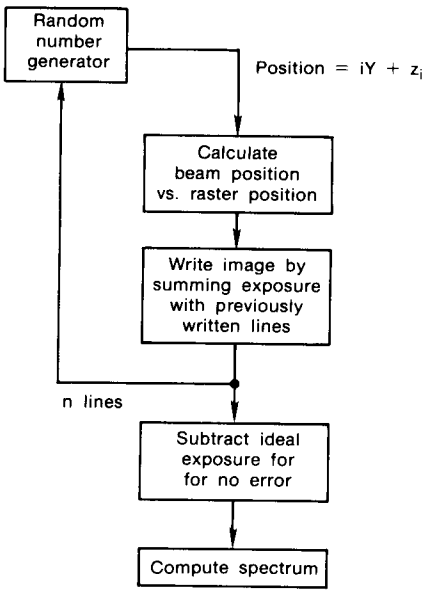

Fig. 7. Diagram of simulation calculation.

Linear Interpolator

The LI refers to a pixel exposure that ideally is a pyramid, and the slow scan profile at the raster position iY is

$$S_i(x) = \begin{cases} 1 - \dfrac{|x - iY|}{Y} & \text{if } (i-1)Y < x < (i+1)Y, \\ 0 & \text{otherwise.} \end{cases} \tag{14}$$

For many applications this spot profile will have advantages over a Gaussian beam. Ideally, the linear interpolator will generate a constant exposure for a constant input, since the $\text{sinc}^2[\text{sinc}(x) = \sin(\pi x)/\pi x]$ reconstruction function [i.e., the Fourier transform of the linear interpolator is a $\text{sinc}^2(u)$] has a value of zero at the frequency $1/Y$. If the Gaussian width is chosen to match the LI reconstruction function at the Nyquist frequency, $w_0 = 1/2Y$, the LI reconstruction function is higher for frequencies below w_0 and lower for frequencies above w_0. The implication of this is better resolution and reduced aliasing.[10,11]

For the case of the LI and iid position errors, the mean value of the exposure is a constant equal to unity, as shown in Theorem 3. This result applies for errors drawn from any probability distribution. No analog of Theorem 3 exists for the Gaussian spot, since it was previously shown that the error function has a nonstationary mean. The immediate corollary is that the error function for the linear interpolator has zero mean at every point. This does not imply that there is no error but that the error is centered about the ideal level taking on both positive and negative values.

The exposure error variance for the LI profile is found in Theorem 5, given by

$$\sigma_v^2(x) = \sum_{i=-\infty}^{\infty} \left\{ \int_{-Y-x}^{Y-x} S^2(x + \alpha_i) p(\alpha_i - iY) d\alpha_i - \left[\int_{-Y-x}^{Y-x} S(x + \alpha_i) p(\alpha_i - iY) d\alpha_i \right]^2 \right\}. \tag{15}$$

Figure 6 shows the error signal variance as a function of position for several position-error values. This variance is nonstationary and periodic at interraster positions, as for the Gaussian spot.

IV. Position-Error Simulation

Analytical results have now been presented that describe the effect of random position errors on the written exposure images. Expressions for the exposure mean and variance as a function of position-error statistics and spot shape have been given. To verify these results and investigate the special case of facet errors for a rotating polygon, we undertook an image simulation effort. Since errors to be addressed were only occurring in the slow scan direction, a 1-D simulation was performed by calculating the exposure for each faster line written in the image. The position of each raster line could then be subjected to a position-error function or random error process with given parameters. A 1-D exposure image of ten raster lines is simulated in this way. Many realizations are simulated by repeating the calculations with different position errors drawn from the same population. Figure 7 shows a diagram of the simulation calculations.

Random Errors

Estimation of the noise power spectrum of the exposure error is complicated because the mean (for the Gaussian spot) and variance are nonstationary. This is because the noise power spectrum amplitude of the random variable $v(x)$ is nonstationary and periodic in the page-scan direction. We can, however, periodically sample the image so that the sampled random process is wide-sense stationary. In addition, if we assume that this sampled process is ergodic, the noise power spectrum can be estimated conventionally. Examination of Figs. 3, 4, and 6 shows that both the mean and variance functions are periodic with period equal to Y.

The exposure error mean and variance, due to their periodic nature, are equal at positions $Y/4, 3Y/4, \ldots$.

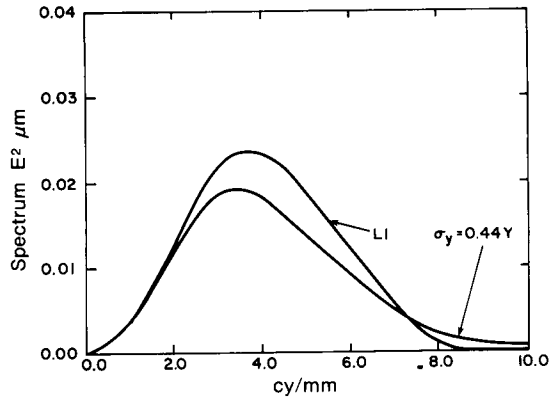

Fig. 8. Simulated exposure error spectra for Gaussian and LI profiles, random errors, $\sigma_z = 1\%$, $Y = 0.1$ mm, as determined at either $y = Y/4$ or $y = 3Y/4$, where the exposure variance takes on its mean value.

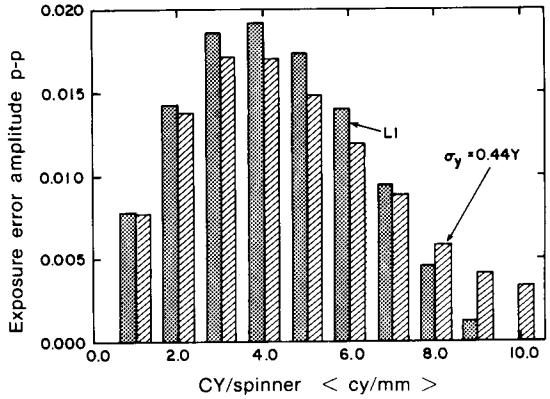

Fig. 9. Simulated exposure error spectra for Gaussian and LI profiles, periodic errors, $\sigma_z = 1\%$, $Y = 0.1$ mm, as might be generated by a mirrored polygonal deflector.

This allows us, under the previous assumptions, to estimate the noise power spectrum for frequencies up to $1/Y$. The resulting spectrum estimate (Fig. 8) agrees well with that derived in Appendix C and given in Eq. (10) with $K = 2$. Note that this noise power spectrum characterizes the exposure fluctuations at specific positions with respect to the raster lines. However, at locations $Y/4$ and $3Y/4$ the variance takes on its average value. Since the noise power spectrum represents the spatial frequency decomposition of the variance, the spectrum calculated for the error process at these points represents a useful average spectrum.

The units of the error noise power spectrum are different from those generally used for spectrum estimation of 2-D noise processes. This is because, although the written exposure image is two-dimensional, it is stochastic in only one dimension since we are addressing the effect of raster line misplacement and not individual pixel misplacement. The spectrum units are, therefore (exposure^2 × distance), instead of (exposure^2 × distance^2) for the Wiener spectrum and in which exposure is energy deposited per unit area on the photoreceptor. The image exposure fluctuations considered are proportional to the underlying line position errors. The calculated spectra shown in Fig. 9 is for 1% position errors. The image noise corresponding to more practical levels (5–20%) can, therefore, be found by simple scaling of the spectra by the square of the error relative to the 1% position error.

Periodic Facet-Position Errors

In the previous sections we have analyzed the effect of position errors in terms of the characteristics of the errors themselves, whether very low frequency, random, or periodic. We have avoided modeling specific physical causes, since these will vary with different designs and technologies used. One important type of periodic error is not included in the above analysis and is best understood in the context of the primary cause, polygon facet-angle variations. Exposure beams deflected by a rotating polygon are subject to errors in both fast and slow scan directions.[4] As above, we will analyze only errors that cause image noise in the slow scan direction, i.e., pyramidal or facet-to-axis angle errors. These cause variations in the raster pitch, except that now they are repeated, since the polygon rotates as the image is written. So for a polygon spinner with, say, ten reflecting facets, the effect of a single facet error is repeated every ten raster lines.

We start by assuming that each individual facet of a spinner is subject to a small random pyramidal error. As with the previous analysis, this will cause a line-position error at the written image. The difference for this case is that the output exposure is no longer a (nonstationary) stochastic process but is a periodic signal dependent on the facet errors of the particular spinner used. Put another way, the periodic noise due to a given spinner will be the result of a single realization (or group of n realizations for an n-facet spinner) of the underlying random facet-error process.

The working equations needed to calculate the exposure are identical to those for the previous random-error case:

$$v(x) = \sum_{i=-\infty}^{\infty} [S_i(x) - S_i(x + z_i)],$$

$$z_i = z_{n+i}, \tag{16}$$

where n is the number of facets per polygon.

The resulting exposure fluctuations were calculated via the simulation. The facet errors were assumed to be random and normally distributed, so in the simulation each raster line was shifted by an appropriate position error for each facet of the spinner. Ten facets per spinner were assumed. For a single polygon spinner, ten errors were drawn, and the resulting exposure fluctuations were computed. The spatial frequency components were then identified by computing a discrete Fourier transform. Each spinner has its unique associated periodic image noise; however, the ensemble of spinners was analyzed by repeating the above calculations for many realizations of the facet errors. The population of spinners (and facet errors) was quantified by calculating the noise spectrum of the error signal. Since the exposure error is periodic, ow-

ing to rotation of the spinner down the image, the noise spectrum is discrete with components at multiples of the rotation frequency $1/nY$ for an n-facet spinner. This was done for both Gaussian and linear interpolator beam shapes, as shown in Fig. 9. Since the spectra are discrete, the units are merely exposure. We plot the peak-to-peak amplitude (four times the Fourier modulus) to be consistent with the previous analysis of periodic position errors.[2] The results of the simulation compare with the results of the analytic approach used for the case of random raster-position error. A linear interpolator demonstrates a similar response to periodic facet errors as the Gaussian profile. The periodic peak-to-peak amplitude spectrum is shown for 1% position errors. The amplitudes corresponding to other values of position errors are obtained by simple proportional scaling of those in Fig. 9.

The agreement between the calculations of periodic and random raster-position errors is not surprising, as the periodic position errors locally are random errors. Also, since the periodic and random errors form independent classes of errors, the two classes of error can be examined independently. The effect of the two types of error can be easily put in terms of the density-error index.

V. Density-Error Index

The preceding analysis can be related to the resulting optical density fluctuations in the written image. For an integrated measure, the pointwise statistics of the analysis can be averaged over a raster unit to give an effective value of rms density noise. This averaging is advantageous, as the nonstationary random processes can be replaced by stationary statistics. The density-error index is

$$\text{density error} = \gamma[\log(C + C\sigma_v) - \log(C - C\sigma_v)]$$

$$= \gamma \log\left(\frac{1 + \sigma_v}{1 - \sigma_v}\right), \tag{17}$$

where C is the exposure level, σ_v is the average standard deviation of exposure over a raster unit, and γ is the gradient of the photosensitive $D - \log E$ characteristic curve at the mean exposure. Note that this is two times the average rms density fluctuations and similar to that used by Bestenreiner *et al.*[2]

For random errors this measure is clearly statistical, as the errors may result in density variations exceeding the index values. The measure does provide a useful design aid. The calculation of the above measure shows that the density errors, although nearly identical, are uniformly less for the Gaussian spot. Figure 10 shows the density-error index as a function of the standard deviation of the raster error.

The importance of this is that, although the image quality of a laser-writing system can be improved by using a laser spot shape other than the normal Gaussian, one does not incur substantially greater sensitivity to raster position errors. Recall that the Gaussian profile selected, $\sigma_y = 0.44$ raster units, is the profile that best matched the MTF characteristics of the optimal spot profile. As previously mentioned, a wider Gaussian spot will have reduced average variance and hence a lower density-error index. However, the writing scheme has reduced contrast and lower signal-transfer capability.

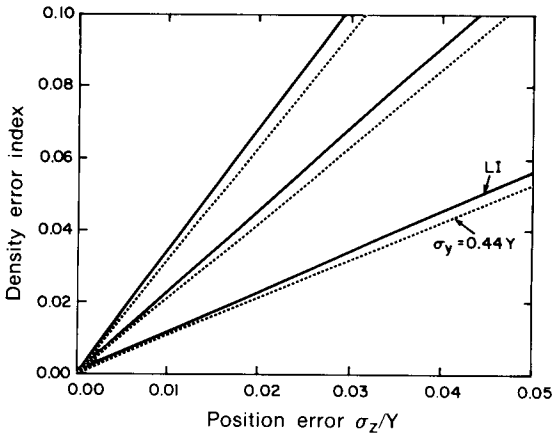

Fig. 10. Density error index for Gaussian and LI profiles due to random variation in the placement of the scan-line centers with respect to the intended raster locations. $\gamma = 1$, 2 and 3.

We can also calculate the output density noise power spectrum via the characteristic curve of the recording medium:

$$PS_D(f) = \gamma^2(\log_{10}e)^2 PS_E(f). \tag{18}$$

This is based on the usual assumption of small exposure variations about the mean exposure, which applies in our case of continuous-tone printing. Figures 11 and 12 show the density noise spectra for the random- and facet-error cases for recording materials with $\gamma = 1$. The spectra values are proportional to both σ_z and f, as can be seen from Eq. (B5). From Eq. (18) it is seen that the spectra of the written image are proportional to the square of the γ of the recording material, which will vary with mean exposure.

VI. Conclusions

Since a laser writer represents a final stage in an imaging system, its requirements are usually described by signal-transfer and noise properties. For example, the requirements for the granularity of the recording materials can be expressed in terms of an output SNR[12] or noise equivalent number of quanta.[13] In general, these metrics are most appropriate for the description and specification of 2-D stochastic noise degradation. For 1-D single-frequency periodic fluctuations, results of sine-wave or square-wave visibility threshold experiments are often used to set noise requirements.

Current levels of position errors in laser writers lead to image banding fluctuations that are both visible and unacceptable for some high-quality applications. Reduction of line position errors in laser printers often requires increased complexity and cost. It is intended that the analysis presented here provides a tool for the integration of this aspect of mechanical design into the imaging performance requirements for hard copy dis-

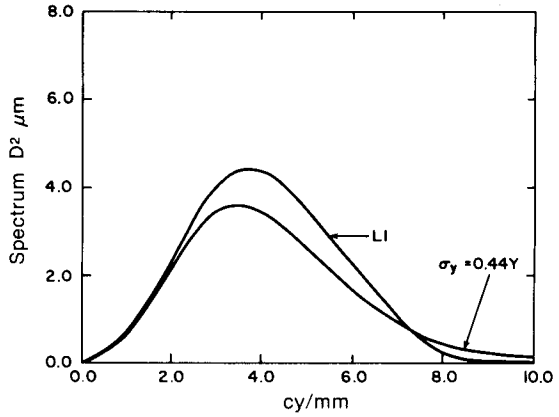

Fig. 11. Simulated density error spectra for Gaussian and LI profiles, random errors, $\sigma_z = 0.01Y$, $Y = 0.1$ mm, exposed onto photosensitive material with $\gamma = 1$.

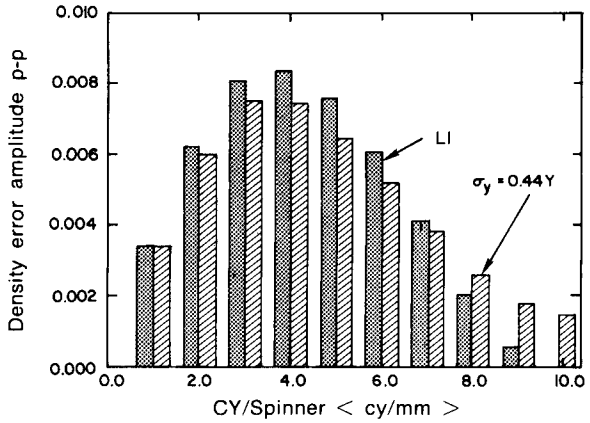

Fig. 12. Simulated density error spectra for Gaussian and LI profiles, periodic errors, $\gamma = 1$, $\sigma = 0.01Y$, $Y = 0.1$ mm.

play. The image noise is described not only in terms of the position error statistics but also the reconstruction (interpolation) scheme. By expressing the stochastic and periodic image artifacts in terms of spectral density and spatial frequency, their effect can be understood in terms of the image signal bandwidth and other noise sources. This is analogous to the analysis of aliasing in the context of the system MTF.

One-dimensional random and periodic image fluctuations that result from the position errors addressed here can be thought of as artifacts such as rastering. For these types of image degradation, the most useful approach is to require that the magnitude of the artifacts be below some practical visibility criterion. These requirements are most stringent if the image to be written is a constant field, as typical for parts of a continuous-tone image.

The random polygon-facet errors result in periodic image fluctuations of several frequencies at various unknown phase angles. Nevertheless, the use of visibility threshold curves (for single-frequency periodic noise) seems apt, particularly at low spatial frequencies. Our analysis of random position errors has identified 1-D nonstationary stochastic exposure fluctuations. Since these are neither 2-D random nor single-frequency periodic, metrics developed for these types of noise must be applied with care. It is advisable, as with other such artifacts, to augment the analysis with simulation experiments. The 1-D random image noise, however, can be described by an average 1-D power spectral density and will appear as random bands or stripes in the image. For components at low spatial frequencies, these may appear similar to the 1-D periodic noise and, therefore, be specified similarly.

It is our pleasure to acknowledge the numerous contributions to the development of our ideas from colleagues in these Laboratories, especially R. Firth, D. Haas, E. Muka, and J. Sullivan. We would also like to acknowledge significant and timely suggestions and advice from R. Shaw.

Appendix A: Mathematical Derivations and Proofs

The following are the theorems and proofs referred to in the body of this paper. Theorems 1 and 2 assume the writing spot to be a Gaussian profile, whereas the rest of the results assume a linear interpolator for the writing pixel. The line-placement errors are assumed to be independent and identically distributed. These errors are referred to as random errors as opposed to periodic errors. The notation used in the following is

$E(\ )$ = expected value operator,
σ_y^2 = variance of the Gaussian writing spot in the slow scan direction,
z_i = random variable denoting the ith-raster line-position error,
Y = intended raster line spacing.

In all cases the maximum value of any individual pixel is assumed to be unity, and the input signal is assumed constant and set to unity. These assumptions do not restrict the generality of the results.

THEOREM 1: If the raster line errors are iid with a Gaussian probability density function having zero mean and variance σ_z^2, the expected exposure error at position x is given by

$$\mu_v(x) = \sum_{i=-\infty}^{\infty} \exp\left[-\frac{(x - iY)^2}{2\sigma_y^2}\right] - \frac{\sigma_y}{(\sigma_y^2 + \sigma_z^2)^{1/2}} \exp\left[-\frac{(x - iY)^2}{2(\sigma_z^2 + \sigma_y^2)}\right]. \quad \text{(A1)}$$

PROOF: By definition, the expected error at point x is given by

$$\mu_v(x) = \sum_{i=-\infty}^{\infty} E[S_i(x) - S_i(x + z_i)]$$

$$= \sum_{i=-\infty}^{\infty} \{S_i(x) - E[S_i(x + z_i)]\},$$

where z_i is the position error of raster line i. Thus it is sufficient to determine the expected value of $S_i(x + z_i)$. By application of first principles,

$$E[S_i(x+z_i)] = \frac{1}{\sqrt{2\pi}\sigma_z}\int_{-\infty}^{\infty}\exp\left[-\frac{(x-iY+z_i)^2}{2\sigma_y^2}\right]$$

$$\times\exp\left(-\frac{z_i^2}{2\sigma_z^2}\right)dz_i$$

$$= \frac{\sigma_y}{(\sigma_y^2+\sigma_z^2)^{1/2}}\exp\left[-\frac{(x-iY)^2}{2(\sigma_y^2+\sigma_z^2)}\right]. \quad \text{(A2)}$$

The result immediately follows.

Expression (A1) is used extensively in calculation of the variance of the exposure error.

THEOREM 2: If the raster line errors are iid with a Gaussian probability density function having zero mean and variance σ_z^2, the variance of the exposure error at a position x is given by

$$\sigma_v^2 = \sum_{i=-\infty}^{\infty}\left\{\frac{\sigma_y}{(2\sigma_z^2+\sigma_y^2)^{1/2}}\exp\left[-\frac{(x-iY)^2}{2\sigma_z^2+\sigma_y^2}\right]\right.$$

$$\left.-\frac{\sigma_y^2}{\sigma_y^2+\sigma_z^2}\exp\left[-\frac{(x-iY)^2}{\sigma_y^2+\sigma_z^2}\right]\right\}. \quad \text{(A3)}$$

PROOF: By assumption, the errors at each raster line are independent, so the exposure error at a point x is the sum of independent random variables:

$$v_i(x) = S_i(x) - S_i(x+z_i).$$

Hence, the variance of the exposure error is the sum of the variances of the random variables $v_i(x)$.[14] Let $\sigma_i^2(x)$ be the variance of the random variable $v_i(x)$. By definition,

$$\begin{aligned}\sigma_i^2(x) &= E[v_i^2(x)] - \mu_i^2(x)\\ &= E\{[S_i(x) - S_i(x+z_i)]^2\} - \mu_i^2(x)\\ &= S_i^2(x) - 2S_i(x)E[S_i(x+z_i)]\\ &\quad + E[S_i^2(x+z_i)] - \mu_i^2(x),\end{aligned}$$

where $\mu_i(x)$ is the mean value of the random variable $v_i(x)$ and is determined by a tedious but direct computation. The expected value of $S_i(x+z_i)$ is Eq. (A2). The expected value of $S_i^2(x+z_i)$ is

$$\frac{\sigma_y}{(2\sigma_z^2+\sigma_y^2)^{1/2}}\exp\left\{-\frac{(x-iY)^2}{2\sigma_z^2+\sigma_y^2}\right\}.$$

By combining the separate terms and performing some algebraic manipulations, the resulting expression becomes

$$\sigma_v^2(x) = \frac{\sigma_y}{(2\sigma_z^2+\sigma_y^2)^{1/2}}\exp\left[-\frac{(x-iY)^2}{2\sigma_z^2+\sigma_y^2}\right]$$

$$-\frac{\sigma_y^2}{\sigma_y^2+\sigma_z^2}\exp\left[-\frac{(x-iY)^2}{\sigma_y^2+\sigma_z^2}\right].$$

The desired quantity then results by summing over the individual components.

The remaining theorems assume the spot shape represents a linear interpolator. This is given by Eq. (14) in the text and is repeated here:

$$S_i(x) = \begin{cases}1 - \dfrac{|x-iY|}{Y} & \text{if } (i-1)Y < x < (i+1)Y\\ 0 & \text{otherwise.}\end{cases}$$

THEOREM 3: If the raster-line positioning errors are iid with a probability density function $p(z)$, the expected value of the exposure at any point for a constant input is constant. Moreover the mean exposure error is zero.

PROOF: By applying the definition of expectation and the spot profile, the expected exposure can be written as

$$\begin{aligned}\text{expected exposure} &= \sum_{i=-\infty}^{\infty}E[S_i(x+z_i)]\\ &= \sum_{i=-\infty}^{\infty}\int_{-\infty}^{\infty}S_i(x+z_i)p(z_i)dz_i.\end{aligned}$$

By assuming the sum is absolutely convergent and the random variables z_i are changed to iid, the order of the summation can be rearranged.

Also, let $w_i = -iY - x$. Therefore,

$$\sum_{i=-\infty}^{\infty}\int_{w_i}^{w_{i-1}}\left(1+\frac{w_i-z_i}{Y}\right)p(z_i)dz_i$$

$$+\int_{w_{i+1}}^{w_i}\left(1-\frac{w_i-z_i}{Y}\right)p(z_i)dz_i$$

$$=\sum_{i=-\infty}^{\infty}\int_{w_i}^{w_{i-1}}\left(1+\frac{w_i-z_i}{Y}\right)p(z_i)dz_i$$

$$+\int_{w_i}^{w_{i-1}}\left(1-\frac{w_i-z_i}{Y}\right)p(z_i)dz_i$$

$$=\int_{-\infty}^{\infty}p(z_i)dz_i = 1.$$

The expected exposure error is the difference in the expected exposure with positioning errors and the exposure without positioning errors. Since the exposure without positioning errors is unity, the difference is zero.

COROLLARY 4: The expected value of the exposure at a point x when the jth raster line is omitted is given by

$$1 - \int_{-(j+1)Y-x}^{-(j-1)Y-x}S_j(x+\lambda)p(\lambda)d\lambda.$$

PROOF: This immediately follows from Theorem 3.

THEOREM 5: If the raster-line positioning errors are iid with a probability density function $p(z)$, the variance at any point is given by

$$\sigma_v^2(x) = \sum_{i=-\infty}^{\infty}\left\{\int_{-Y-x}^{Y-x}S^2(x+\alpha_i)p(\alpha_i - iY)d\alpha_i\right.$$

$$\left.-\left[\int_{-Y-x}^{Y-x}S(x+\alpha_i)p(\alpha_i-iY)d\alpha_i\right]^2\right\}.$$

PROOF: For a fixed raster position x, the individual position errors independently contribute to the total exposure error. As in the proof of Theorem 2, it is sufficient to add the variances of the random variables to determine the variance of the exposure error. However, algebraically it is simpler to compute the variance directly without immediately applying the independence of the individual error terms:

$$\text{Let } v(x) = \sum_i [S_i(x) - S_i(x + z_i)],$$

then

$$\begin{aligned}\sigma_v^2(x) &= E[v^2(x)] - \mu^2(x)\\ &= E[v^2(x)],\end{aligned}$$

where $\mu(x)$ = mean exposure error = 0 (Theorem 3).

By expanding the expression and applying Theorem 3 to three of the resulting summations, and then by use of Corollary 4, we obtain

$$\begin{aligned}E[v^2(x)] &= -1 + E\left[\sum_i \sum_j S_i(x + z_i)S_j(x + z_j)\right]\\ &= E\left[\sum_i S_i(x + z_i)^2\right]\\ &\quad - E\left[\sum_i S_i(x + z_i)\right]\int_{-(i+1)Y-x}^{-(i-1)Y-x} S_i(x + \lambda_i)p(\lambda_i)d\lambda_i\\ &= \sum_i \int_{-Y-x}^{Y-x} S^2(x + \alpha_i)p(\alpha_i - iY)d\alpha_i\\ &\quad - \int_{-Y-x}^{Y-x} S(x + \alpha_i)\\ &\quad \times\left[\int_{-(i+1)Y-x}^{-(i-1)Y-x} S_i(x + \lambda_i)p(\lambda_i)d\lambda_i\right]p(\alpha_i - iY)d\alpha_i.\end{aligned}$$

By a change of variable, using the definition of the spot profile and the property that the random variables are iid, the result follows.

Appendix B: Mean Exposure Error

This Appendix provides an analytic derivation to the spectral model of the exposure noise generated by random positioning errors. The model is actually a special case of the results of the analytic model, although the model captures the most useful part of the analysis. The analysis assumes the spot shape to be a Gaussian profile. The case for the linear interpolator can be handled similarly.

From Theorem 1 of Appendix A the mean of the error is given by the expression

$$\mu_v(x) = \sum_{i=-\infty}^{\infty}\left\{S_i(x) - \frac{\sigma_y}{\sqrt{\sigma_y^2 + \sigma_z^2}}\exp\left[\frac{(x - iY)^2}{-2(\sigma_y^2 + \sigma_z^2)}\right]\right\}.$$

Since $\mu_v(x)$ is a periodic function with period equal to the spacing between adjacent raster lines (i.e., Y), it can be expanded as a Fourier series of the form

$$\mu_v(x) = a_0 + \sum_{l=1}^{\infty} a_l \cos\left(\frac{2\pi l}{Y}x\right), \tag{B1}$$

where

$$a_0 = \frac{1}{Y}\int_{-\frac{Y}{2}}^{\frac{Y}{2}} \mu_v(x)dx, \tag{B2}$$

$$a_l = \frac{2}{Y}\int_{-\frac{Y}{2}}^{\frac{Y}{2}} \mu_v(x)\cos\left(\frac{2\pi l}{Y}x\right)dx. \tag{B3}$$

It can be easily verified that $a_0 = 0$. To find a_l we note that

$$\begin{aligned}a_l &= \frac{2}{Y}\int_{-\frac{Y}{2}}^{\frac{Y}{2}} - \frac{\sigma_y}{\sqrt{\sigma_y^2 + \sigma_z^2}}\sum_{i=-\infty}^{\infty}\exp\left[\frac{(x - iY)^2}{-2(\sigma_y^2 + \sigma_z^2)}\right]\cos\left(\frac{2\pi l}{Y}x\right)dx\\ &\quad + \frac{2}{Y}\int_{-\frac{Y}{2}}^{\frac{Y}{2}}\sum_{i=-\infty}^{\infty}\exp\left[\frac{(x - iY)^2}{-2\sigma_y^2}\right]\cos\left(\frac{2\pi l}{Y}x\right)dx\\ &= a_{1l} + a_{2l}.\end{aligned}$$

Since $\mu(x)$ is an absolutely convergent series (with probability 1), the terms may be rearranged in any manner. In particular, the series may be broken into two pieces, and the coefficients of the Fourier series can be computed by individually integrating with respect to each of the pieces and then adding the results. Let the second part of the expression be given by the series

$$\begin{aligned}a_{2l} &= \frac{2}{Y}\sum_{i=-\infty}^{\infty}\int_{-\frac{Y}{2}}^{\frac{Y}{2}}\exp\left[\frac{(x - iY)^2}{-2\sigma_y^2}\right]\cos\left(\frac{2\pi l}{Y}x\right)dx\\ &= \frac{2}{Y}\int_{-\infty}^{\infty}\exp\left(\frac{x^2}{-2\sigma_y^2}\right)\cos\left(\frac{2\pi l}{Y}x\right)dx,\end{aligned}$$

where we have interchanged the order of the summation and the integration. The resulting summation of finite integrals can be converted to a single integral with the region of intergation over the entire line. Indeed, the expression is simply

$$a_{2l} = \frac{2\sqrt{2\pi}\sigma_y}{Y}\exp\left(\frac{-2\sigma_y^2 l^2\pi^2}{Y^2}\right), \tag{B4}$$

where the latter result is derived using integral tables. Similarly, a_{1l} is found to be

$$a_{1l} = -\frac{2\sqrt{2\pi}\sigma_y}{Y}\exp\left[\frac{-2\pi^2 l^2(\sigma_y^2 + \sigma_z^2)}{Y^2}\right], \tag{B5}$$

Finally,

$$\begin{aligned}a_l &= a_{1l} + a_{2l}\\ &= \frac{2\sqrt{2\pi}\sigma_y}{Y}\exp\left(\frac{-2\pi^2\sigma_y^2 l^2}{Y^2}\right)\left[1 - \exp\left(\frac{-2\pi^2 l^2\sigma_z^2}{Y^2}\right)\right],\end{aligned} \tag{B6}$$

We define $R(f)$ as the Fourier transform of the spot $S(x)$, and since a Gaussian spot of radius σ_y has a Gaussian Fourier transform,

$$R(f) = \sqrt{2\pi}\sigma_y \exp(-2\pi^2\sigma_y^2 f^2).$$

Equation (B6) may be recast as

$$a_l = \frac{2}{Y} R\left(\frac{l}{Y}\right)\left[1 - \exp\left(-\frac{2\pi^2 l^2 \sigma_z^2}{Y^2}\right)\right]. \quad \text{(B7)}$$

An approximation can be made by expanding the exponential in the expression and ignoring all terms beyond the second degree. By doing this, the approximation becomes

$$a_l \approx 4\pi^2 \sigma_z^2 \left(\frac{l^2}{Y^3}\right) R\left(\frac{l}{Y}\right). \quad \text{(B8)}$$

This is the desired result, since from (B1) and (B8) with $l = 1$,

$$\mu_v(x) \cong 4\pi^2 \left(\frac{\sigma_z}{Y}\right)^2 \frac{1}{Y} R\left(\frac{1}{Y}\right) \cos\left(\frac{2\pi x}{Y}\right).$$

Appendix C: Derivation of Amplitude Spectral Model

This Appendix derives the amplitude spectral model previously presented. The noise power spectral model was given the form

$$PS(f) = [k\sigma_z f R(f)]^2 \quad \text{(C1)}$$

where k = constant,
σ_z = standard deviation of the position errors,
f = spatial frequency, and
R = Fourier transform of the beam profile in the page scan direction.

Assuming the spot is a sufficiently smooth function, the value of the spot can be expressed by a Maclaurin series as

$$\text{spot}(x + z) = \sum_{n \geq 0} \frac{\text{spot}^{(n)}(x) z^n}{n!}. \quad \text{(C2)}$$

[$\text{spot}^{(n)}(x)$ is the nth derivative.] Hence the error function is given by

$$V(x,z) = \text{spot}(x + z) - \text{spot}(x) = \sum_{n \geq 1} \frac{\text{spot}^{(n)}(x) z^n}{n!}. \quad \text{(C3)}$$

By a Fourier transformation of Eq. (C3) we obtain $M(f)$, the modulus

$$M(f) = R(f)\left|\sum_{n \geq 1} \frac{(2\pi j f z)^n}{n!}\right|$$
$$= R(f)[2(1 - \cos(2\pi f z)]^{1/2}$$
$$\sim |2fzR(f)|. \quad \text{(C4)}$$

[Equivalently, we could have performed the approximation in Eq. (C3) by ignoring all but the first term of the expression.]

Assuming the position error z is a random variable with a Gaussian distribution, the expected value of Eq. (C4) is

$$E[M(f)] = \sqrt{2\pi}\sigma_z f R(f). \quad \text{(C5)}$$

The power spectrum $PS(f)$ takes the form of the square of $M(f)$, which is the desired result.

The value of the constant in Eq. (C5) is $k = \sqrt{2\pi}$, whereas the estimated value found by the simulation was $k = 2$. This is a reasonable agreement, if we consider the approximations used in Eq. (C4) and the errors from the qualitative method used in the body of the text.

References

1. J. C. Urbach, T. S. Fisli, and G. K. Starkweather, "Laser Scanning for Electronic Printing," Proc. IEEE **70,** 597 (1982).
2. F. Bestenreiner, U. Geis, J. Helmberger, and K. Stadler, "Visibility and Correction of Periodic Interference Structures in Line-by-Line Recorded Images," J. Appl. Photogr. Eng. **2,** 86 (1976).
3. F. M. Lowry and J. J. Depalma, "Sine-Wave Response of the Visual System. II. Sine-Wave and Square-Wave Contrast Sensitivity," J. Opt. Soc. Am. **52,** 328 (1962); see also F. L. Van Nes and M. A. Bouman, "Spatial Modulation in the Human Eye," J. Opt. Soc. Am. **57,** 401 (1967).
4. D. Kessler and R. V. Shack, "Dynamic Optical Tests of a High-Speed Polygon," Appl. Opt. **20,** 1015 (1981).
5. P. J. Brosens, "Scanning Accuracy of the Moving-Iron Galvanometer Scanner," Opt. Eng. **15,** 95 (1976).
6. T. Tenada, T. Sato, S. Tatuoka, M. Aiko, and H. Masuko, "High-Quality Laser Color Television Display," J. Soc. Motion Pict. Telev. Eng. **82,** 470 (1973).
7. F. O. Huck, N. Halyo, and S. K. Park, "Aliasing and Blurring in 2-D Sampled Imagery," Appl. Opt. **19,** 2174 (1980).
8. W. K. Pratt, *Digital Image Processing* (Wiley, New York, 1978), Chap. 4.
9. W.-H. Lee, "Method for Converting a Gaussian Laser Beam into a Uniform Beam," Opt. Commun. **36,** 469 (1981).
10. L. A. Ray, "Optimal Pixel and Spot Shape for Laser Imaging," in *Proceedings, SPSE Second International Congress, Advances in Non-Impact Printing Technology*, Arlington, VA (1984), pp. 136–138.
11. J. R. Sullivan, "Fourier Masks for Modification of Laser Recording Spots," in *Proceedings, SPSE Second International Congress, Advances in Non-Impact Printing Technology*, Arlington, VA (1984), pp. 48–51.
12. J. H. Altman and H. J. Zweig, "Effect of Spread Function on Storage of Information on Photographic Emulsions," Photogr. Sci. Eng. **7,** 173 (1963).
13. R. Shaw and P. D. Burns, "Noise Requirements for the Recording Medium of a Laser Printing Device," in *Proceedings, SPSE Second International Congress, Advances in Non-Impact Printing Technology*, Arlington, VA (1984), pp. 127–130.
14. W. Feller, *An Introduction to Probability and Its Applications, Vol. 1* (Wiley, New York, 1968).